Electrochemical Properties of Electrospun Metal-Organic Frameworks (MOFs) Nanofibers as Novel Hybrid Electrode Materials

Subhajit Sarkar
Universiti Malaya
Noordini Mohamad Salleh
Universiti Malaya
Özay Eroğlu
Mugla Sıtkı Koçman University
Fatma Kuru
Mugla Sıtkı Koçman University
Afike Ayça Özen
Mugla Sıtkı Koçman University
Sema Aslan
Mugla Sıtkı Koçman University
Hulya Kara Subasat
Mugla Sıtkı Koçman University
Siti Nadiah Abdul Halim (nadiahhaim@um.edu.my)
Universiti Malaya

Research Article

Keywords: Metal–organic frameworks (MOFs), nanofiber electrodes, polyvinylidene fluoride, carbon-paste electrodes, electrochemical studies, electrospinning

Posted Date: October 13th, 2023

DOI: https://doi.org/10.21203/rs.3.rs-3374962/v1

Additional Declarations: No competing interests reported.

Abstract

This research focuses on exploring the electrochemical properties of UiO-66 and MOF-199 (metal-organic framework (MOFs)-based electrodes, in the form of nanofibers fabricated along with PVDF through electrospinning techniques on a pencil graphite electrode (PGE). SEM images obtained showed the UiO66/PVDF and MOF199/PVDF nanofibers have different morphology affected by addition of different MOF into the PVDF polymers with mean diameters of 750 nm and 750 nm respectively. TGA results indicated that the nanofibers possess a high thermal degradation temperature, exceeding 400°C, which indicates increased material robustness compared to the pure MOFs alone. Mechanical strength analysis of the nanofibers revealed contrasting mechanical properties. UiO66/PVDF exhibited a strain percentage of 309.4 but a relatively low stress value of 0.4299 MPa. On the other hand, MOF199/PVDF displayed a high stress value of 3.718 MPa but a lower strain percentage of 46.34%. Electrochemical studies were conducted on the electrodes; MOFs/PVDF/PGE and the MOFs/GCPE (carbon paste electrodes) to compare MOFs' standalone electrochemical properties. Different scan rates were applied to all electrodes in the interval of 5, 20, 50 100, and 250 $mVsec^{-1}$ and the best C_s values were obtained from the MOF199/PVDF/PGE nanofiber electrode. Furthermore, prolonged charge-discharge measurements were executed using a scan rate of 100 mV/sec across 200 cycles for all electrodes. This phase was extended to 3000 cycles exclusively for the MOF199/PVDF/PGE nanofiber electrode. The outcomes underscored remarkable stability, particularly notable in the case of the MOF199/PVDF/PGE nanofiber electrode, highlighting its potential as a reliable energy storage electrode.

1. Introduction

Metal–organic frameworks (MOFs) are novel materials that are becoming scientific and technological importance owing to their stability, large internal surface area and porous nature [1–3]. These characteristics allow them to be suitable materials for applications such as catalysis, gas storage, drug delivery, gas vapor separation, luminescence, lithium-ion batteries, water treatment, and carbon dioxide capture, as well as photo- and electrocatalysis [4–6]. However, despite their numerous advantages, the appearance of the materials in the form of solids limits their integration into many technologies. This creates a huge drawback that affects their applicability for industrial and commercial uses [7]. Hence, integration of MOFs and polymers have been taken as an effort to combine the properties of MOFs and polymers to enhance the utility of MOFs to different environments and conditions [8–12].

Many integration techniques were reported to fabricate the MOF-polymer nanofiber materials; such as encapsulation, impregnation, infiltration, solid grinding, and coprecipitation [13]. Different types of preparation method can produce different properties and hence improve the applicability of the materials [14]. Compared with the other composite fabrication processes, electrospinning technique is a superficial and flexible route to fabricate MOF-polymer nanofiber materials with microporous and nanofibrous morphology [15–18]. This technique serves as a proper platform to implant MOFs into the polymer nanofibers while retaining their original features. MOFs can be trapped and confined in the polymer chain, and this indirectly exposes more MOFs' active spots. A wide range of promising MOFs nanofibers have been reported to date, and their potential use in various technological fields has been investigated. [19–22]

MOFs-based nanofibers have garnered significant interest and attention as promising candidates for energy storage devices. These nanofibers possess unique and advantageous properties that make them suitable for

various energy storage applications [23–24]. MOFs-based nanofibers have been incorporated into flexible and lightweight electrode architectures, as well as electrolytes making them suitable for integration into wearable and portable energy storage devices [25–28]. This flexibility enables the development of energy storage solutions that can conform to various shapes and surfaces, expanding their application in diverse fields, including wearable electronics and medical devices. In general, the utilization of MOFs-based nanofibers as energy storage devices is able to unlock their potential for next-generation energy storage solutions [29–30].

In this context, the primary goal of our study is to create a nanofiber material with exceptional thermal conductivity by combining metal-organic frameworks (MOFs) with polymers. Previous research has provided encouraging yet limited findings regarding the proton conductivity of MOF-polymer nanofibers, specifically focusing on UiO-66 and MOF-199 [31–32]. To leverage their potential for various applications, we independently incorporated UiO-66 and MOF-199 with polyvinylidene fluoride (PVDF), taking advantage of their remarkable mechanical properties, thermal stability, and chemical characteristics [33–34].

Our approach involved optimizing the synthesis method for these nanofibers on pencil graphite electrodes using electrospinning techniques, followed by an assessment of their electrochemical properties. Additionally, we explored the standalone potential of the MOFs by modifying them with carbon paste electrodes, considering the benefits of ease of fabrication, renewability, excellent stability, and reproducibility.

2. Experimental

2.1. Materials

The reagents; zirconium(IV) chloride (Acros, USA), copper(II) nitrate (Sigma-Aldrich, USA), terephthalic acid (Sigma-Aldrich, USA), trimesic acid (Acros, USA), N,N-dimethylformamide (Synerlab, Malaysia), ethanol (R&M Chemicals, U.K.), hydrochloric acid (Merck, USA) are analytical grade and were used without further purification.

2.2. Instrumentation

The production of nanofibers in the polymeric air filter by the electrospinning method was carried out with the "SG1, Spingenix Electrospinning Device".

Fourier Transform Infrared Spectroscopy (FTIR) was used to collect the Infrared spectra by Perkin Elmer Spectrum 400 FTIR/FT-FIR spectrometer (USA).

The crystallinity of MOFs materials was characterized by PANalytical, X'Pert HighScore diffractometer with primary monochromatic high intensity Cu-Kα (λ = 1.54184) radiation in the scanning range of 5° to 40°.

The morphology and surface topography of the produced nanofibers were made with the Field Emission Scanning Electron Microscope (FESEM); JSM-7600F Quanta 250 SEM device at IZTECH Materials Research Center. Diameters of nanofibers were analyzed using ImageJ (NIH, Bethesda, MD) software on SEM images (10000X).

Thermogravimetric analysis for the nanofiber filter was performed with Perkin Elmer Thermal Analyzer under nitrogen (2.5 bar, 10 mL/min) atmosphere at a heating rate of 10°Cmin^{-1}, at a temperature range of 30–700°C.

Mechanical strength analysis was performed using TA Instruments Q800 DMA (Dynamic Mechanical Analysis). The tests were carried out at 37ºC by applying a force of 0.1N/min. Tensile and tear strength tests were performed to determine the mechanical properties of the filter material. SDL Testometric M350–10 CT device was used for both tests. Tests were carried out to reveal the mechanical durability properties of the produced air filter. The samples were cut into strips of filter material to perform the tests. The width of the samples used in the rupture tests was 10 mm, and the width of the samples used in the tear tests was 50 mm. ISO 527-1 and ISO 527-3 standards were used for tear strength tests, and ISO 6383-1 standards were used for tear strength tests.

The electrochemical experiments (CV) were recorded with a triple electrode system (Gamry Potentiostat-Galvanostat) including platinum foil as counter, Ag/AgCl as reference and the examined electrode as working. Electrolytes were 0.01 M $K_3[Fe(CN)_6]$ including PBS solution for the characterizations.

2.3. Synthesis

2.3.1. Synthesis of UiO-66

0.116 g of terephthalic acid was dissolved in 10 ml of DMF. Simultaneously, 0.117 g of zirconium (IV) tetrachloride was dissolved in 6 ml of DMF mixed with HCl in a 5:1 ratio. The two solutions were then combined in the same flask and subjected to reflux and stirring at 85°C for a duration of 23 hours. As a result, a white precipitate formed in the mixture. To isolate the product, centrifugation was performed, followed by drying in a hot air oven at 70°C for 24 hours. The process yielded a white powder with a 0.198 g yield (93%) [35].

2.3.2. Synthesis of MOF-199

0.3045g (3.0 mmol) of trimesic acid and 0.114g (1.1 mmol) of copper (II) nitrate are dissolved in a minimal amount of ethanol and deionized water (DI) respectively at room temperature. The solutions are then combined in a single beaker and stirred at temperatures ranging from 70°C to 100°C for approximately 15–30 minutes. Once a light blue precipitate forms, the mixture is allowed to cool and reduce. The product is subsequently isolated through filtration, yielding a light blue powder with the yield of 0.252 g (85.8%) [36].

2.3.3. Preparation of MOFs/ PVDF Solution

PVDF with a weight percentage of 16% was dissolved in a mixture of DMF and acetone in a 7:3 ratio under stirring at 50°C for 6 hours. Subsequently, 0.12 g of grounded MOFs were introduced to 5 ml of PVDF solution to create mixtures with concentrations of 15% (w/w%). These mixtures were stirred for one hour to ensure the formation of homogeneous blends before proceeding with the preparation of electrospun nanofiber electrodes.

2.3.4. Preparation of MOFs/ PVDF/ PGE Nanofiber electrodes

The preparation of MOFs/PVDF/PGE nanofiber electrodes involved the utilization of an electrospinning device. This device relies on three crucial parameters: the solution flow rate, the applied voltage, and the distance between the collector and the syringe. During the nanofiber production, the applied voltage ranged from 17 to 20 kV, the flow rate was set at 1.25 ml/min, and the distance between the collector and the syringe was maintained at 20 cm. A rod-shaped like collector was used and rotated about an axis parallel to the E field [37].

2.3.5. Preparation of MOFs/ GCPE electrodes

The UiO-66/GCPE electrode was prepared by mixing 80% glassy carbon graphite powder with 20% mineral oil and adding 15% UiO-66. On the other hand, the MOF-199/GCPE electrode was prepared by mixing 80% glassy carbon graphite powder with 20% mineral oil and adding 5% MOF-199.

3. Results and discussion

3.1. MOF Synthesis

The synthesized MOFs; UiO-66 and MOF-199 were confirmed via FT-IR and PXRD techniques.

3.1.1 FTIR Measurement

The FT-IR spectra of the synthesized UiO-66 and MOFS are represented in Table 1. Based on the results, it can be concluded that the correspondence peaks agree with values reported in the literature [35–36].

Table 1
IR stretching frequencies (cm^{-1}) of Terephthalic acid (TPA), Trimesic acid (TCA) and respective MOFs.

Assignments	TPA	MOF-199	TMA	UiO-66
(H_2O)	-	-		
ν(O-H)	2811	-	2791	3221
ν(C = O)	1680	1636	1712	1708
ν_{asym}(COO-)	1574	1587	1449	1558
ν_{sym}(COO-)	1407	1370	1399	1382
ν(C-O)	1280	1247	1270	1273
$\Delta_\nu(\nu_{asym} - \nu_{sym})$	167	217	50	176

3.1.2 PXRD Analysis

The comparison of the PXRD patterns of the synthesized MOFs (red) and the ones simulated from CIFs (blue) is shown in Fig. 1. The patterns match respectively, indicating that the synthesized bulk materials have high crystallinity and are representative of single crystals. However, it is worth mentioning that the characteristic peak of MOF-199 (at 2θ = 6.9) was attributed to the difference in the copper (II) precursor. [38].

3.2 Characteristics of MOFs/PVDF/PGE nanofiber electrodes.

3.2.1 SEM Analysis

The SEM analysis findings indicate that the nanofibers possess aligned but diffrent morphology without bead effect as depicted in Fig. 2. It was noted that the UiO-66/PVDF nanofibers somehow has churros-like rough surface morphology with diameters ranging from 400–900 nm, whlist MOF199/PVDF nanofibers shows grooves morphology with diameters within the range of 500–1000 nm [39]. Figure 3 demonstrated the distribution graphs

of both nanofibers where the mean diameters of UiO-66/PVDF and MOF199/PVDF nanofibers are 750 nm and 700 nm respectively. These observations suggest that the introduction of diffrent MOFs into PVDF polymers lead to a significant diffrents in terms of morphology and diameters. In terms of porosity, UiO66 shows higher porosity to compare with MOF199/PVDF with voids percetage of 66.62% and 59.04% respectively, shown in Fig. 4. This shows that high porosity nanofibers have higher nanofiber diameter correlated well with literature [40].

3.2.3 Thermogravimetric analysis

To assess the stability of the MOFs/PVDF nanofiber electrodes, their thermal characteristics were investigated and compared with the pristine MOFs as shown in Fig. 5. Both nanofiber materials exhibited three weight loss stages as the temperature increased up to 700°C. A slight reduction was observed in both MOF nanofibers at temperatures higher than 300–380°C, which might be attributed to the degradation of various oxygen-containing functional groups on the nanofibers' surface [41]. The second weight loss, occurring in the range of 380–480°C, could be attributed to the dissociation of nanofiber polymers. Subsequently, both materials experienced further weight reduction at temperatures higher than 480–700°C, possibly due to the collapse of the MOF frameworks. According to our results, the both nanofibers; UiO-66/PVDF and MOF-199/PVDF exhibited similar thermal stabilities. However, it is worth to highlight that degradation temperature of MOFs/PVDF nanofiber electrodes are higher than the MOFs, may be attributed to the interaction with the PVDF polymers. The final ash content of the pristine MOFs and MOFs/PVDF nanofiber remain also almost similar, about 30.53% and 24.03%, respectively, demonstrating that the thermal stability of MOFs was not significantly affected by the nanofibers.

3.2.4 Mechanical Analysis

The analysis of mechanical strength was conducted on MOFs/PVDF nanofibers, revealing two primary characteristics: stress and strain percentage. The results for UiO66/PVDF nanofibers demonstrated high stress, reaching up to 3.7718 MPa, but the strain percentage was relatively low at 46.34%. Conversely, the MOF199/PVDF nanofibers exhibited a lower stress of only 0.4299 MPa, yet displayed a remarkably high strain percentage of 309.4%. In summary, both MOFs/PVDF nanofibers exhibited distinct and contrasting characteristics in terms of mechanical strength, making them suitable for different applications. Results are summarized in Fig. 6.

3.3 Electrochemical Supercapacitance Measurements

The electrochemical behaviours of the newly crafted nanofiber electrodes were assessed through cyclic voltammetry (CV) measurements. Figure 7 illustrates the gradual transformation of the PGE electrode through the application of the nanofiber coating. Additionally, it highlights the effect of incorporating the MOF-199 and UiO-66 in enhancing electrochemical currents. Moreover, individual electrochemical assessments were performed on the MOFs using the GCPE-based composite electrode. Optimal concentrations of MOF-199 and UiO-66 were evaluated at 5%, 10%, and 15% (w/w) MOF levels. Among these, the most favourable current readings were obtained for electrodes containing 15% UiO66/GCPE and 5% MOF199/GCPE. Consequently, these proportions were employed for further supercapacitance measurements, either by incorporating them into the composite carbon electrodes or using PGE electrodes for nanofiber composite electrodes.

Figure 8 shows the electrochemical supercapacitance performances of the MOFs/PVDF/PGE nanofiber and MOFs/GCPE electrodes evaluated in the 0.100 M KOH (pH 7.20) solution at different scan rates. These results illustrate that the CV area increases by increasing scan rate across all electrode types. The best C_s value was obtained from MOF199/PVDF/PGE nanofiber electrodes at 5 $mVsec^{-1}$ with 111.3816 Fg^{-1}. Overall, the results showed that the capacitance of MOFs/PVDF/PGE nanofibers and MOFs/GCPE electrodes decreases with the increment of the scan rates, summarized in Table 2.

Table 2
Table of C_s value of UiO-66/PVDF/PGE, 15% MOF199/PVDF/PGE, UiO66/GCPE and MOF199/GCPE nanofibers at different scan rates.

Scan rate/ $mVsec^{-1}$	Specific capacitances, C_s/ Fg^{-1}			
	UiO66/PVDF/PGE	MOF199/ PVDF/PGE	UiO66/GCPE	MOF199/GCPE
5	0.0169	111.3816	0.00211	0.01440
20	0.0130	71.2432	0.00181	0.00699
50	0.0058	56.8736	0.00121	0.00479
100	0.0107	31.4118	0.00813	0.00370
250	0.0043	40.8451	0.00416	0.00279

Long term charge-discharge measurements were applied with a 100 $mVsec^{-1}$ up to 200 cycle for all prepared electrodes as shown in Fig. 9. The outcomes of these tests have been organized in Table 3 for reference. In the case of UiO66/PVDF/PGE, the C_s value reached 71.4505 mFg^{-1} at the 100th cycle, subsequently stabilizing at 57.3702 mFg^{-1}. Concerning MOF199/PVDF/PGE, the C_s values reached stabilization after the 160th cycle, settling at 97.17 Fg^{-1}, with a trend of continued increment. This implies that further extending the long-term measurement for the MOF199/PVDF/PGE nanofiber electrode could yield even more pronounced stabilization. To validate this hypothesis, we extended the measurements to 3000 cycles, observing a noteworthy long-term C_s recovery of 102.04% between the 250th and 3000th cycles (Fig. 10).

Table 3
The comparison of first and 200th cycles for long term measurements

Scan rate/ $mVsec^{-1}$	UiO66/PVDF/PGE		MOF199/PVDF/PGE		UiO66/GCPE		MOF199/GCPE	
	C_{sp}/Fg^{-1}	Recovery %	C_{sp}/Fg^{-1}	Recovery %	C_{sp}/Fg^{-1}	Recovery %	C_{sp}/Fg^{-1}	Recovery %
1	0.00285	12.58	11.16	21.31	0.00100	100	0.00371	100
20	0.02250	100.02	37.27	71.39	0.00102	101.66	0.00436	117.65
40	0.03860	171.51	52.36	99.99	0.00099	99.15	0.00439	118.37
60	0.05100	226.37	63.55	121.36	0.00102	102.23	0.00466	125.60
80	0.06180	274.31	72.63	138.72	0.00096	96.34	0.00487	131.18
100	0.07140	317.13	80.09	152.97	0.00093	92.73	0.00504	136.01
120	0.05310	235.69	87.25	166.64	0.00091	90.74	0.00553	148.99
140	0.05450	242.22	92.19	176.07	0.00090	89.89	0.00580	156.39
160	0.05550	246.66	97.17	185.58	0.00087	87.49	0.00609	164.07
180	0.05640	250.71	101.24	193.36	0.00085	84.99	0.00620	167.29
200	0.05730	254.63	104.97	200.49	0.00082	82.24	0.00624	168.18

4. Conclusions

In this study, we began by evaluating optimal concentrations of MOF-199 and UiO-66 at levels of 5%, 10%, and 15% (w/w) within nanofiber and carbon-paste electrodes. Among these options, electrodes containing 15% UiO66/PVDF/PGE, 15% MOF199/PVDF/PGE, 15% UiO66/GCPE, and 5% MOF199/GCP exhibited the most favorable current readings. With these proportions identified, we proceeded to delve deeper into chemical and physical characterization, along with detailed supercapacitance measurements.

We confirmed the prepared MOFs through various techniques, including TGA, FTIR, and PXRD, affirming their similarity to literature-based materials. SEM characterization of the nanofibers revealed notable homogeneity within the PVDF polymers, yet distinctive morphologies between the two MOFs. Specifically, UiO66/PVDF/PGE showcased supple stick nanofibers with an average diameter of 750 nm, while MOF199/PVDF/PGE nanofibers exhibited straight stick nanofibers with an average diameter of 700 nm. These morphologies potentially link to TGA outcomes, where UiO-66 displayed lower-temperature degradation compared to MOF199/PVDF nanofibers. This aligns with mechanical studies indicating contrasting mechanical strength between the two materials. Overall, our chemical and physical assessments highlighted the distinct properties of these nanofibers, pointing towards their promising potential for diverse applications.

Electrochemical evaluations unveiled that MOF199/PVDF/PGE demonstrated remarkable potential as a supercapacitor electrode, boasting a capacitance value of 111 F/g. Long-term scans also indicated a stable performance trend.

Collectively, by synthesizing insights from these characterizations, we gained a comprehensive understanding of the MOFs/PVDF/PGE nanofiber electrodes, with a notable focus on the potential of the MOF199/PVDF/PGE nanofiber electrode as an effective candidate for electrode materials.

Declarations

Acknowledgement

The authors would like to acknowledge financial support from Ministry of Higher Education Malaysia (ERGS-2013-1/8984) and TUBITAK 2221-Fellowships for Visiting Scientists and Scientists on Sabbatical Leave Support Program.

Authors' contribution.

SNAH designed , coordinated the research, drafted and finalized the manuscript. SS prepared the MOFs and confirmed their molecular structures. OE and FK carried out the fabrication of nanofibers with detailed analysis. AAO and SA conduct cyclic voltammetry studies. HKS and NMS participated in research coordination. The authors read and approved the final manuscript.

The authors declare that they have no competing interests that could have appeared to influence the work reported in this paper.

Data availability

The data that support the findings of this study are openly available.

Consent for publication

Not applicable.

Ethics approval and consent to participate.

Not applicable.

References

1. D.M. Kabtamu, Y. Wu and F. Li. J. Hazard. Mater. (2020). https://doi.org/10.1016/j.jhazmat.2020.122765.
2. Y. Sakamaki,M. Tsuji, Z. Heidrick, O. Watson, J. Durchman, C. Salmon, S.R. Burgin and M.H. Beyzavi. J. Chem Educ. (2020). https://doi.org/10.1021/acs.jchemed.9b01166
3. A.E. Baumann, D.A. Burns, B. Liu, B. and V.S. Thoi. Commun. Chem. 2 (2019). https://doi.org/10.1038/s42004-019-0184-6
4. V.F. Yusuf, N.I. Malek, S.K. Kailasa. ACS Omega (2022), https://doi.org/10.1021/acsomega.2c05310
5. S.E.M. Elhenawy, M. Khraisheh, F. AlMomani and G. Walker. Catalysts (2020). https://doi.org/10.3390/catal10111293.
6. R. Kuppler, D.J. Timmons, Q.R. Fang, J.R. Li, T.A. Makal, M.D. Young, D. Yuan, D. Zhao, W. Zhuang, H.C. Zhou. Coord. Chem. Rev. (2009). DOI: 10.1016/j.ccr.2009.05.019

7. B. Yeskendir, J.P. Dacquin, Y.Lorgouilloux, C. Courtois, S. Royer and J. Dhainaut. Mater. Adv. (2021). DOI: 10.1039/D1MA00630D.
8. A.K. Bindra, D. Wang, Y. Zhao. Adv. Mater. (2023). https://doi.org/10.1002/adma.202300700.
9. G.W.Peterson, D.T. Lee, H.F. Barton, T.H Epps III, G.N. Parsons, Nat. Rev. Mater. (2021). https://doi.org/10.1038/s41578-021-00291-2
10. T. Kitao, Y. Zhang, S. Kitagawa, B. Wang and T. Uemura. Chem. Soc. Rev. (2017). https://doi.org/10.1039/C7CS00041C.
11. K. Kokado, Polym. J. (2017). https://doi.org/10.1038/pj.2016.122
12. M. Kalaj, M.S. Denny Jr., K.C. Bentz, J.M. Palomba, S.M. Cohen. Angew. Chem (2018) https://doi.org/10.1002/ange.201812655
13. H. Jiang, Y. Feng, M. Chen, Y. Wang. Int. J. Hydrog. Energy (2013). DOI: 10.1016/j.ijhydene.2013.03.044
14. I. Ahmed, S.H. Jhung. Mater.Today (2014). https://doi.org/10.1016/j.mattod.2014.03.002
15. M. Toriello, M. Afsari, H.K.Shon and L.D. Tijing. Membranes (2020). https://doi.org/10.3390/membranes10090204
16. Y. Xu, Y. Wen, W. Zhu, Y. Wu, C. Lin and Z. Wei. Mater. Lett. (2012). DOI: 10.1016/j.matlet.2012.07.076
17. A. Barhoum, K. Pal, H. Rahier, H. Uludag, I.S. Kim and M. Bechelany. Appl. Mater. Today (2019) https://doi.org/10.1016/j.apmt.2019.06.015
18. Y. Chen, M. Shafiq, M. Liu, Y. Morsi and X. Moa, Bioact. Mater. (2020) doi: 10.1016/j.bioactmat.2020.06.023
19. H.I. Adil, M.R. Thalji, S.A. Yasin, I.A. Saeed, M.A. Assiri, K.F. Chong and G.A.M. Ali. RSC Adv. (2022). doi: 10.1039/d1ra07034g
20. M. Liu, N. Cai, V. Chan and F. Yu. Nanomaterials (Basel). (2019). doi: 10.3390/nano9091306
21. Z. Zhai, J. Wang, Y. Sun, X. Hao, B.en Niu, H. Xieand C. Li. Appl. Surf. Sc. (2023). https://www.mdpi.com/2304-6740/11/2/65
22. Y. Liu, H. Lv, Y. Liu, Y. Gao, H.Y. Kim, Y. Ouyang, D.G. Yu. Mater.Today (2022). https://doi.org/10.1016/j.mtchem.2022.100974
23. Y. Yan, X. Liu, J. Yan, C. Guan and J. Wang. Energy & Environ. Mater. (2020). https://doi.org/10.1002/eem2.12146
24. J. Liu, S. Min, F. Wang, Z. Zhang. J. Power Sources (2020). https://doi.org/10.1016/j.jpowsour.2020.228347
25. J. Yan, T. Liu, X. Liu, Y. Yan, Y. Huang. Coord. Chem. Rev. (2022). https://doi.org/10.1016/j.ccr.2021.214300
26. R. Vinodh, R.S. Babu, S. Sambasivam, C.V.V.M. Gopi, S. Alzahmi, H.J. Kim, A.L.F. de Barros, I.M. Obaidat. Nanomaterials (2022). https://doi.org/10.3390/nano12091511
27. M.Z. Iqbal and U. Aziz. J. Energy Storage (2022). https://doi.org/10.1016/j.est.2021.103823
28. K. Zhang, K.O. Kirlikovali, Q.V. Le, Z. Jin, R.S. Varma, H.W. Jang, O.K. Farha and M. Shokouhimehr. ACS Appl. Nano Mater. (2020). https://doi.org/10.1021/acsanm.0c00702
29. S. Mallakpour, F. Sirousa and C.M. Hussain. New J. Chem., (2021). https://doi.org/10.1039/D1NJ01302E
30. Y. Dou, W. Zhang, A. Kaiser. Adv. Sc. (2019) https://doi.org/10.1002/advs.201902590
31. J. Annamalai, P. Murugan, D. Ganapathy, D. Nallaswamy, R. Atchudan, S. Arya, A. Khosla, S. Barathi, A.K. Sundramoorthy. Chemosphere (2022). https://doi.org/10.1016/j.chemosphere.2022.134184
32. V.S. Naragund, P.K. Panda, Emergent Mater. (2022). https://doi.org/10.1007/s42247-022-00350-6

33. C.V. More, Z. Alsayed, M.S. Badawi, A.A. Thabet, P.P Pawar, Environ. Chem. Lett. (2021). https://doi.org/10.1007/s10311-021-01189-9.
34. M.J. Katz, Z.J. Brown, Y.J. Colón, P.W. Siu, K.A. Scheidt, R.Q. Snurr, J.T. Hupp and O.K. Farha. Chem. Commun. (2013). https://doi.org/10.1039/C3CC46105J.
35. Tranchemontagne, D. J., Hunt, J. R., Yaghi, O. M. Tetrahedron (2008). https://doi.org/10.1016/j.tet.2008.06.036.
36. T.V.N. Thi, C.L.L., T.C. Hoang, T. Nguyen, T.H. Bui, P.H.D. Nguyen and T.P.P. Thi. Adv. Nat. Sci.: Nanosci. Nanotechnol. (2013). doi:10.1088/2043-6262/4/3/035016.
37. A.E. Mamuk C. Kocak, S. Aslan and D.B. Altuntas. Appl. Energy Mater. (2022).
38. W. Liu, C. Huang and X. Jin. Nanoscale Res. Lett. (2014), https://doi.org/10.1186/1556-276X-9-350.
39. M.M. Elnashar, M., & Karakuş, S. (Eds.). (2023). Biocomposites - Recent Advances. IntechOpen. doi: 10.5772/intechopen.104003
40. R.A.O. Bernal, R.O. Olekhnovich, M.V. Uspenskaya, Polymers (2023). https://doi.org/10.3390/polym15092037
41. J.C.C Yeo, D. Kai, C.P. Teng, E.M.J.R Lin, B.H. Tan, Z. Li Z., & He, C. ACS Appl. Polym. Mater. (2020). https://doi.org/10.1021/acsapm.0c00786

Figures

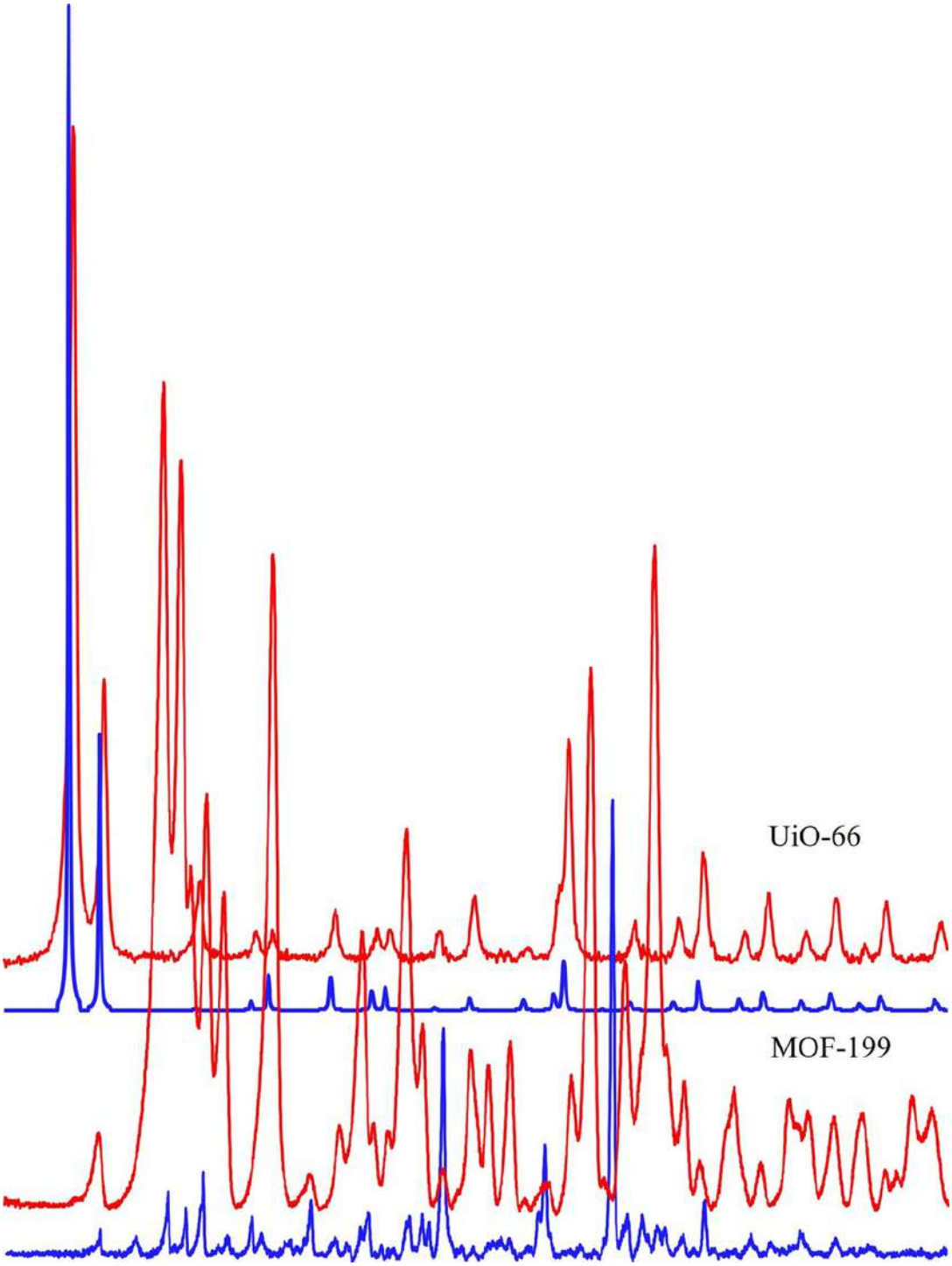

Figure 1

PXRD pattern of experimental (red) and simulated from CIFs (blue).

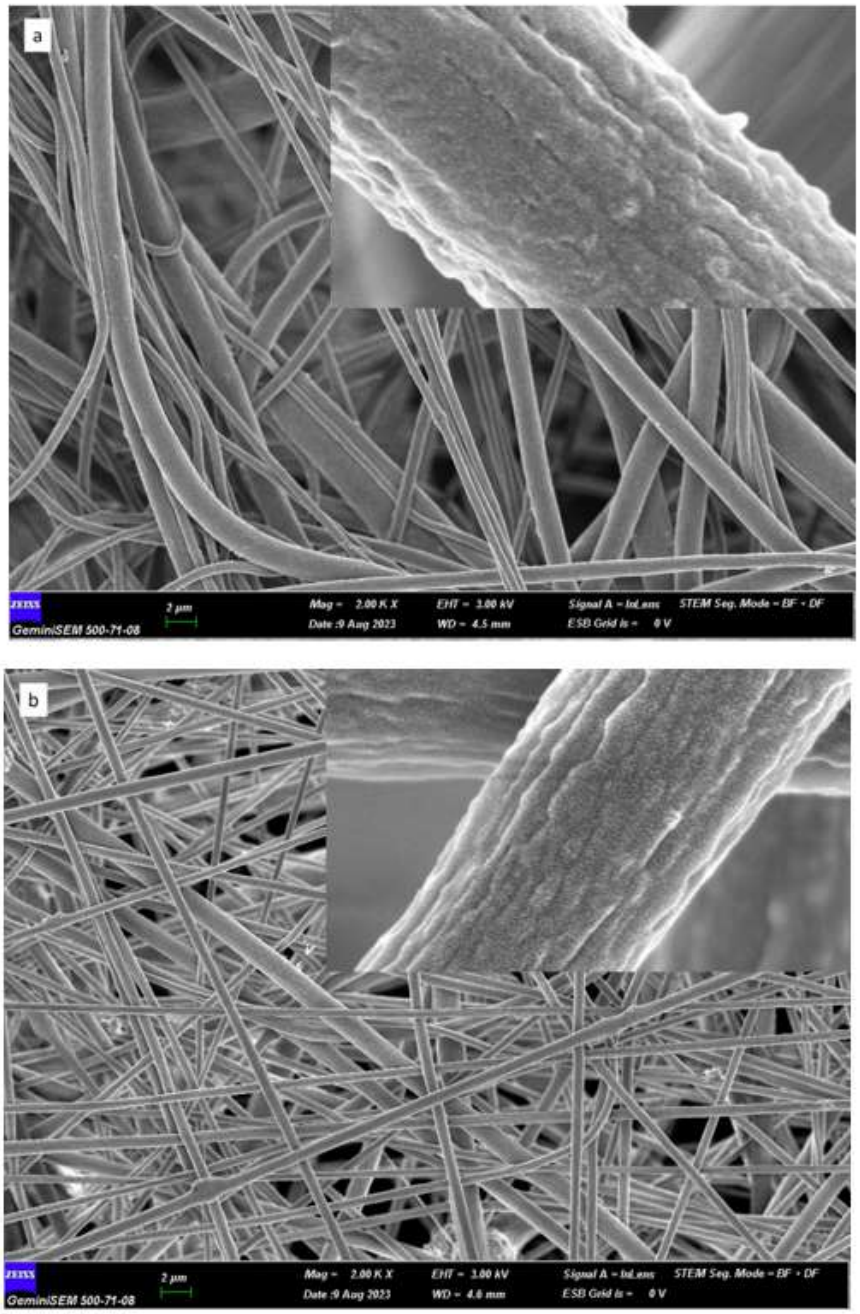

Figure 2

Morphology of fibers at different magnification levels; (a) UiO66/PVDF (b) MOF199/PVDF.

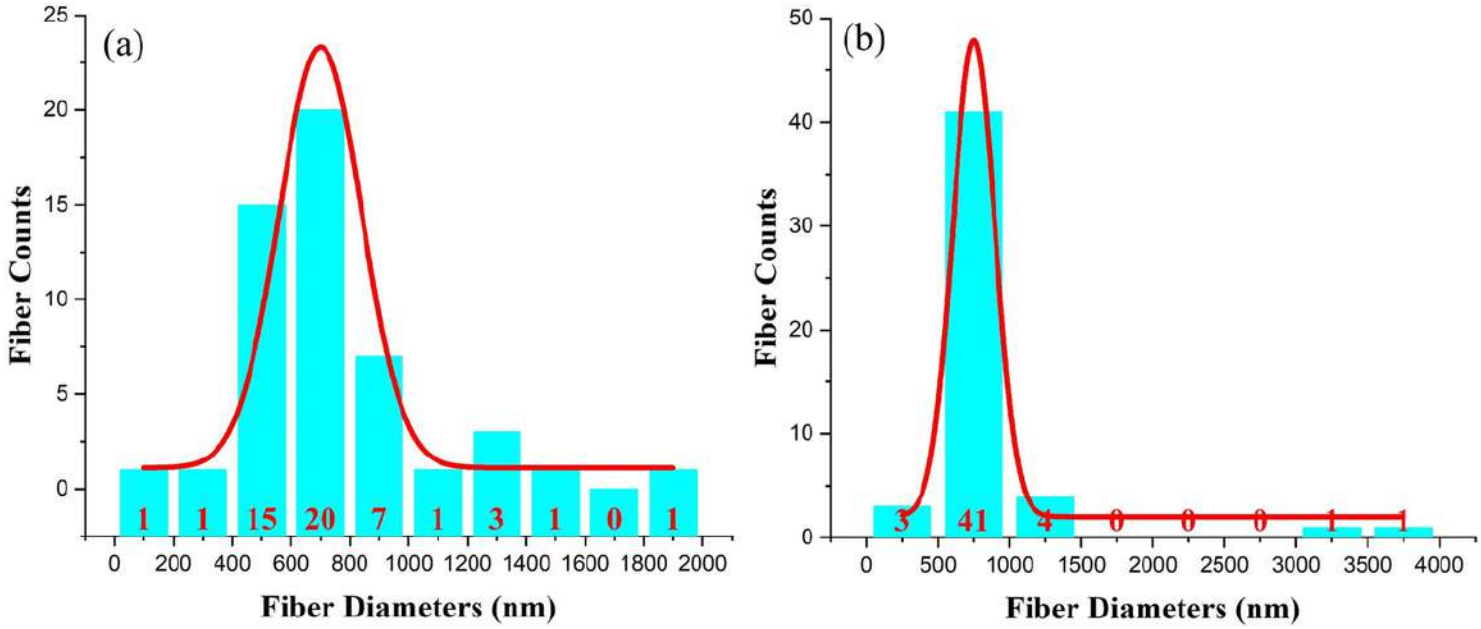

Figure 3

Distribution graphs of (a) UiO66/PVDF and (b) MOF199/PVDF nanofibers.

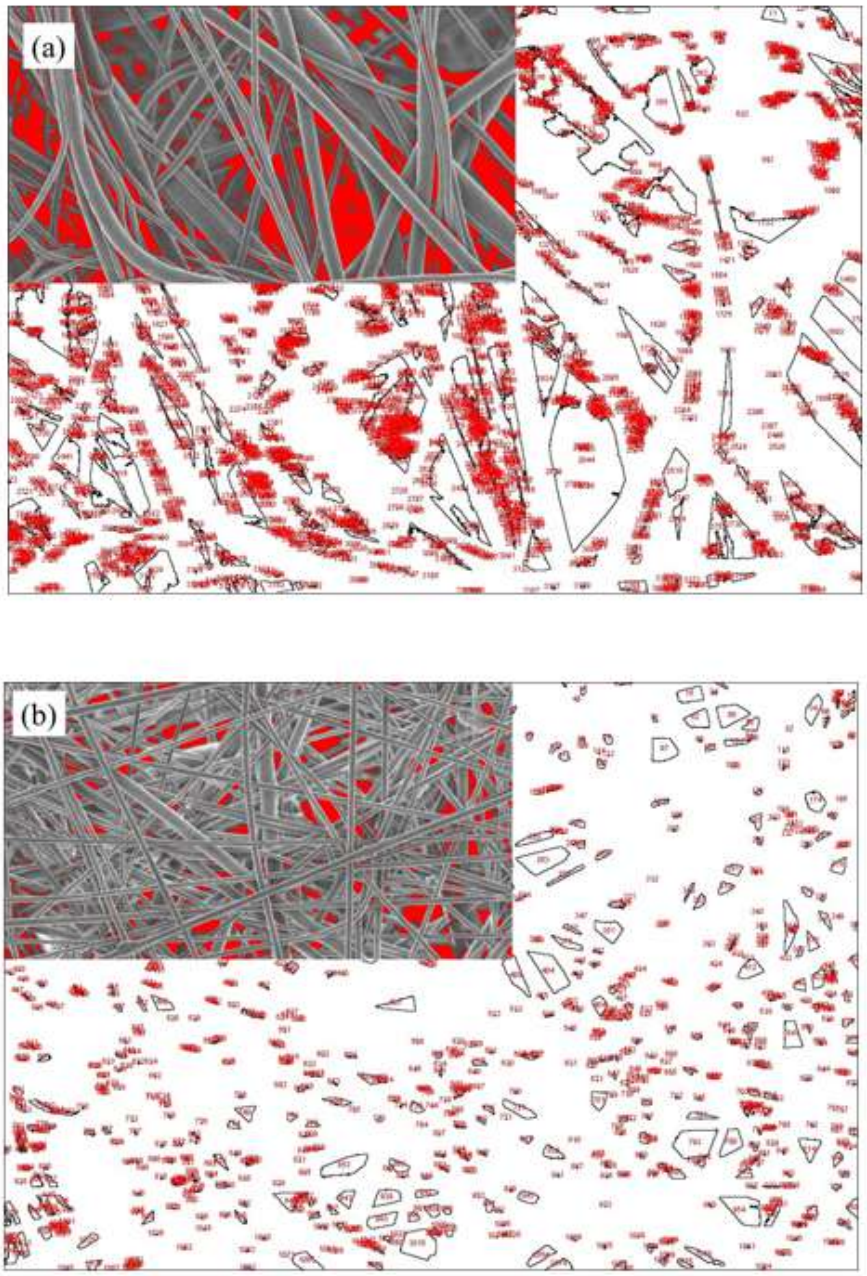

Figure 4

Overview of voids in a) UiO66/PVDF and (b) MOF199/PVDF nanofibers.

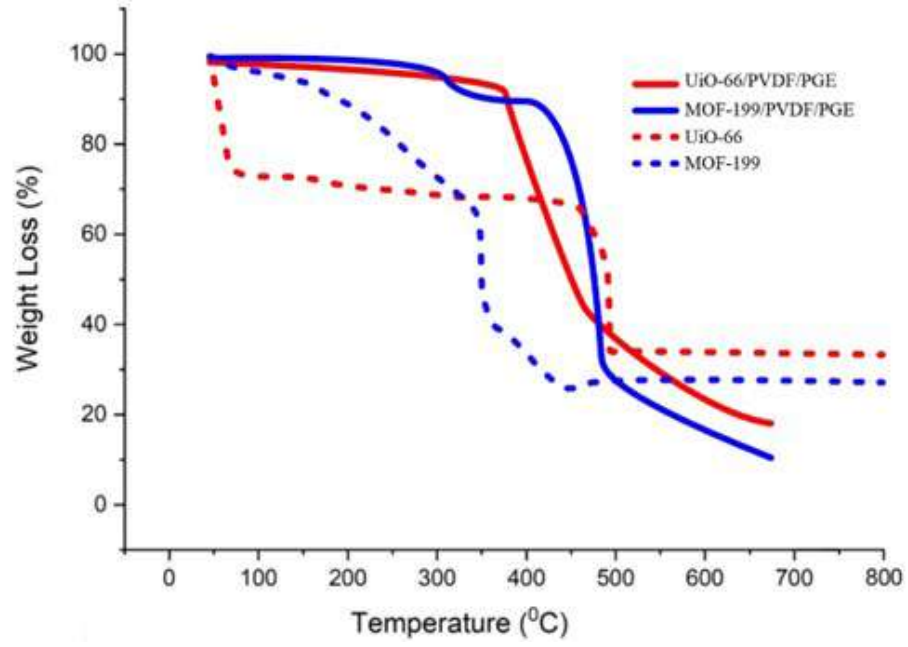

Figure 5

TGA Results for MOFs/PVDF nanofibers

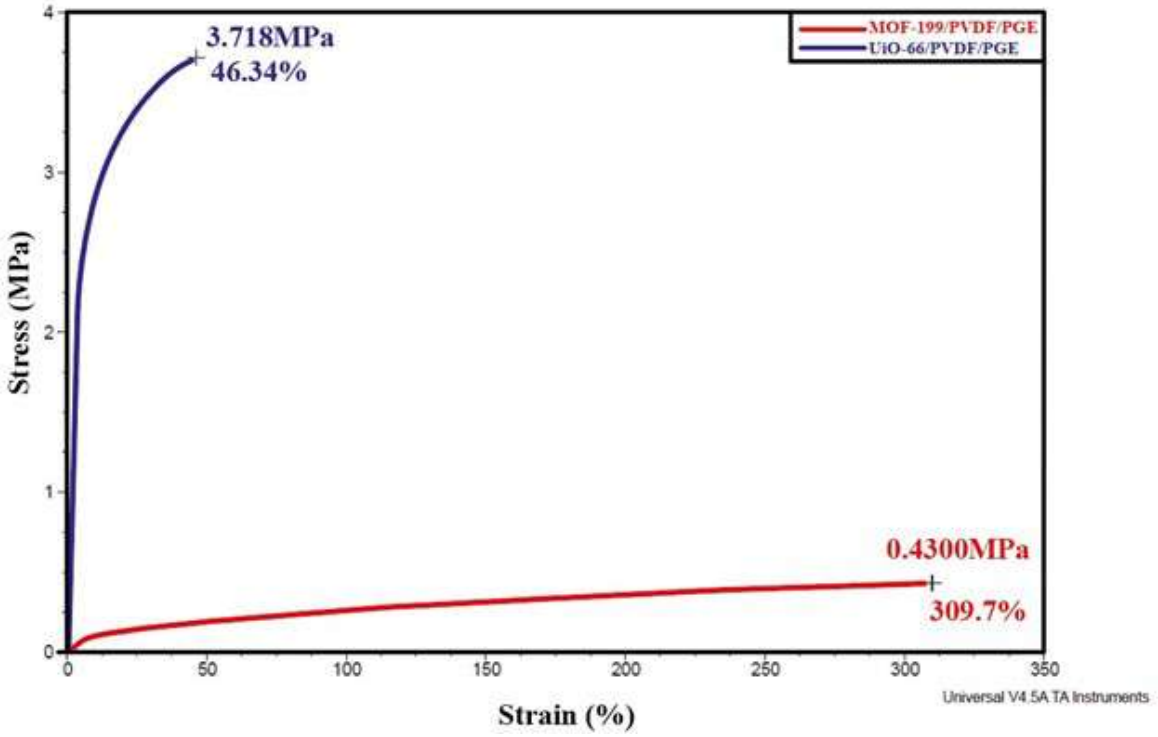

Figure 6

Mechanical Analysis Results for MOFs/PVDF nanofibers.

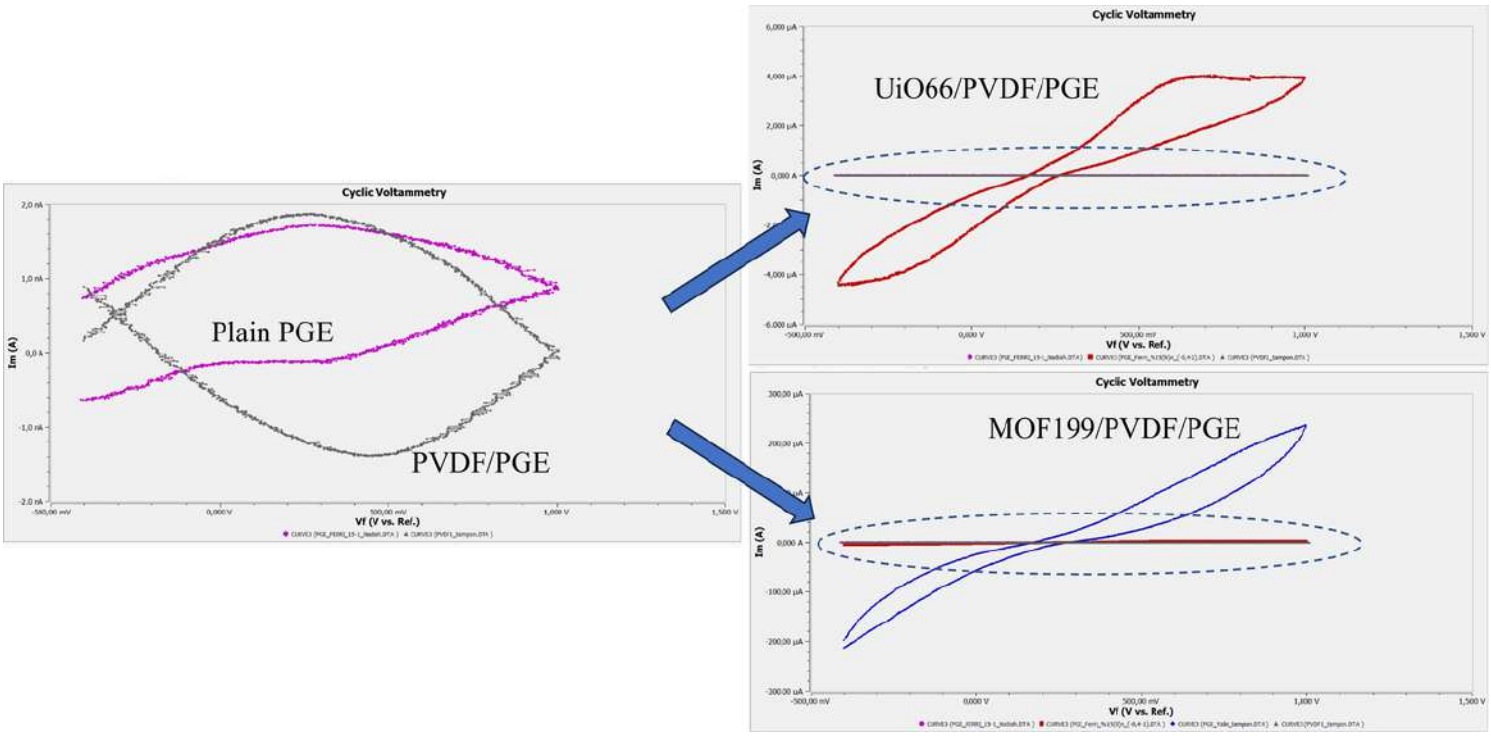

Figure 7

This picture highlights the effect of incorporating the MOF199 and UiO66 MOFs in enhancing electrochemical currents.

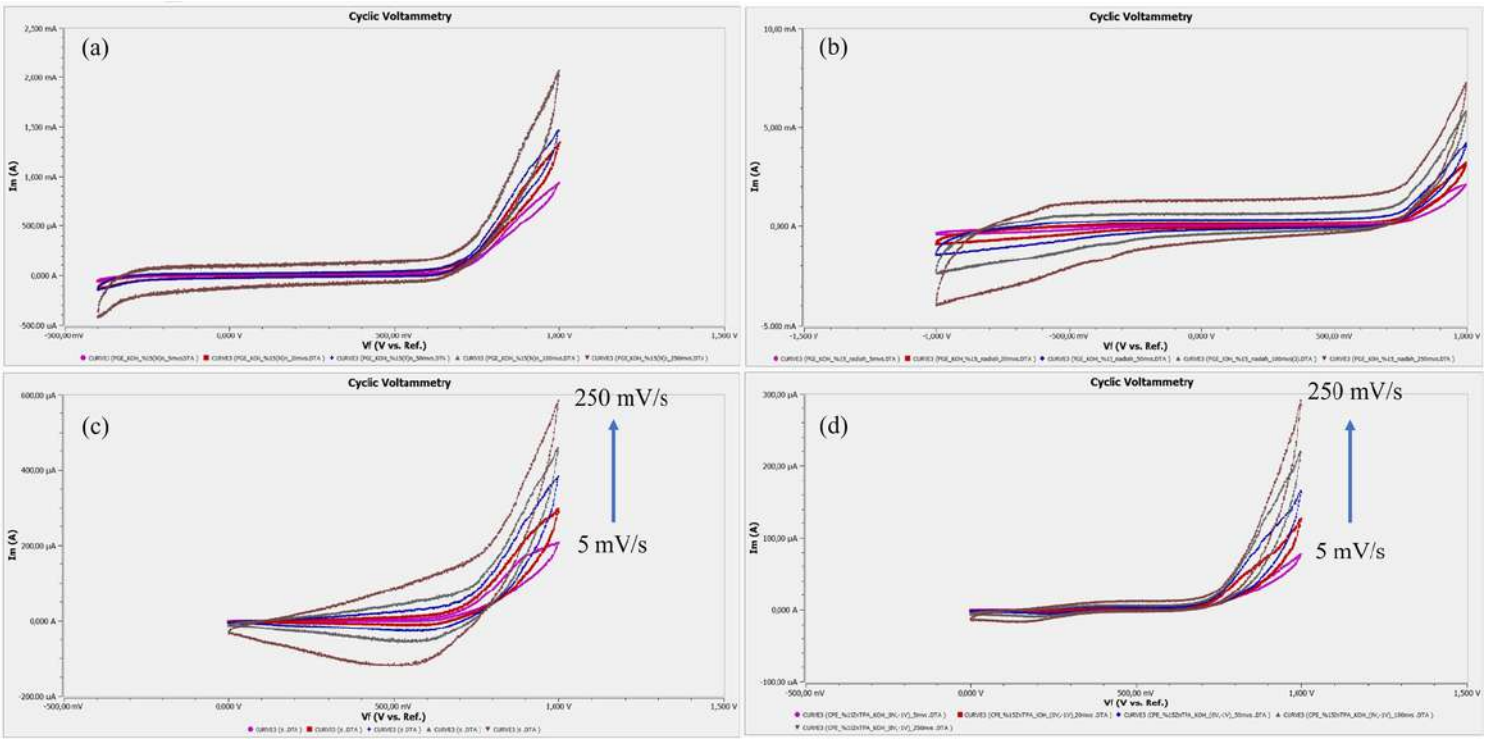

Figure 8

C_s curves of (a) UiO66/PVDF/PGE (b) MOF199/PVDF/PGE (c) MOF199/CPE and (d) UiO66/CPE electrodes at increasing scan rates in 0.1 M KOH solution.

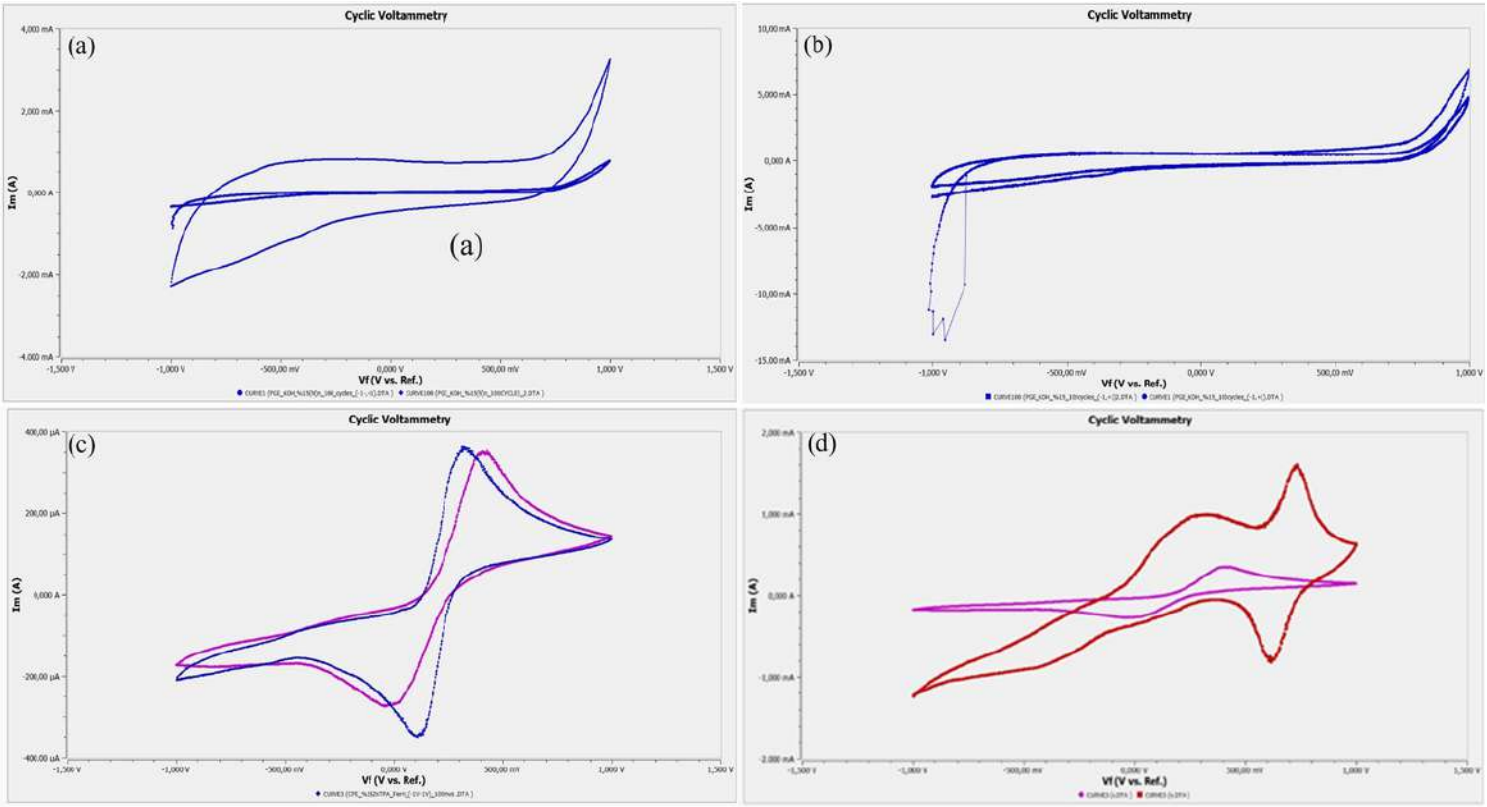

Figure 9

Long-term C_s curves of (a) UiO66/PVDF/PGE (b) MOF199/PVDF/PGE (c) MOF199/CPE and (d) UiO66/CPE electrodes

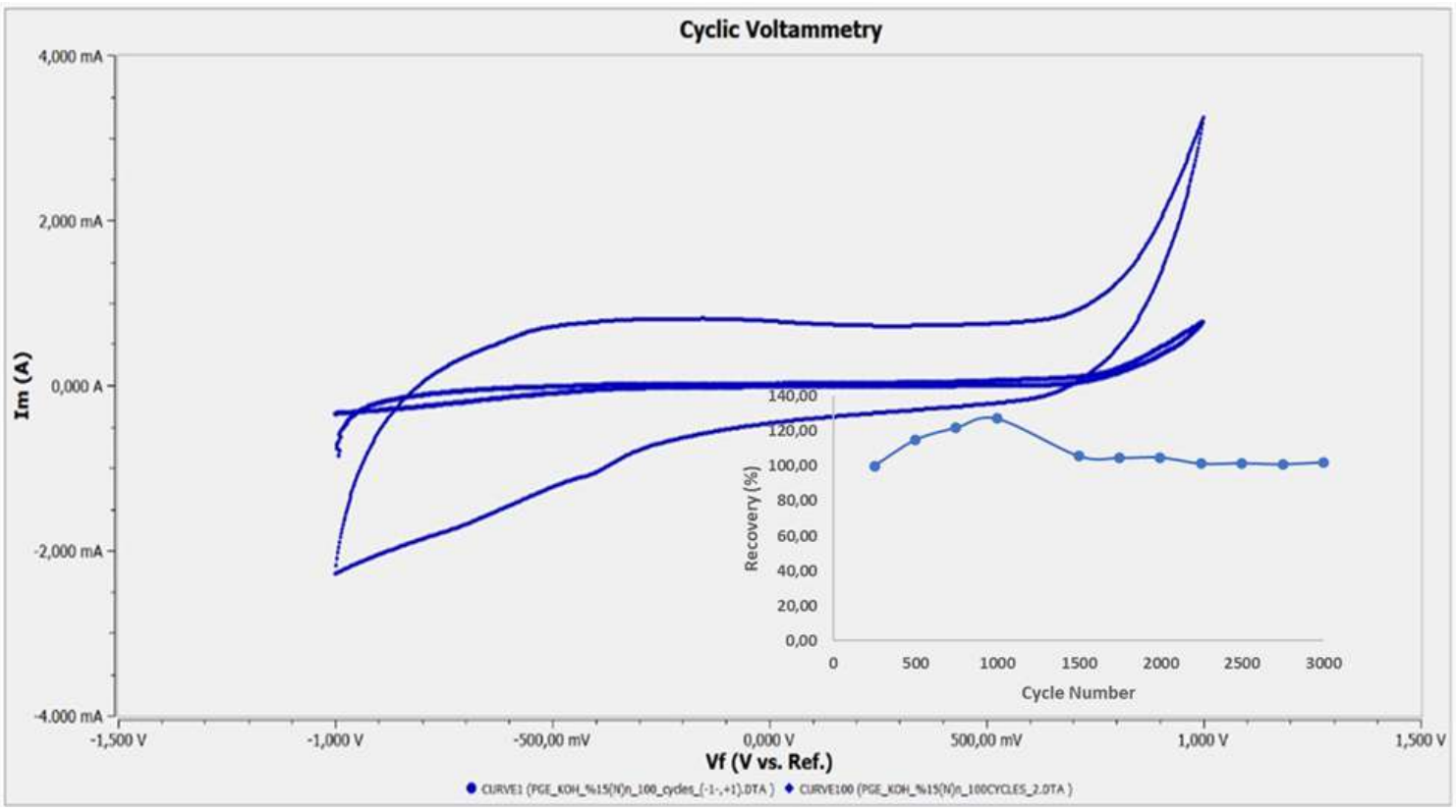

Figure 10

Long-term measuerement for MOF199/PVDF/PGE